Earth and Planetary Science Letters 359-360 (2012) 55–60

Contents lists available at SciVerse ScienceDirect

Earth and Planetary Science Letters

journal homepage: www.elsevier.com/locate/epsl

The influence of fluid properties on the morphology of core turbulence and the geomagnetic field

Michael A. Calkins [a,*], Jonathan M. Aurnou [b], Jeff D. Eldredge [c], Keith Julien [a]

[a] Department of Applied Mathematics, University of Colorado, Boulder, CO 80309, USA
[b] Department of Earth and Space Sciences, University of California, Los Angeles, CA 90095, USA
[c] Department of Mechanical and Aerospace Engineering, University of California, Los Angeles, CA 90095, USA

ARTICLE INFO

Article history:
Received 8 June 2012
Received in revised form
26 September 2012
Accepted 8 October 2012
Editor: T. Spohn
Available online 7 November 2012

Keywords:
Earth's core
geodynamo
convection
turbulence
material properties

ABSTRACT

Here we investigate the effects of fluid properties on the morphology and dynamics of convection in the Earth's outer core. The results of two quasi-geostrophic convection simulations are carried out at comparable convective velocities for fluids in which the ratio between the kinematic viscosity and thermal diffusivity (the Prandtl number, Pr) is 0.1 and 10. The $Pr=0.1$ case is representative of thermal convection in a liquid metal, whereas the $Pr=10$ case is representative of chemical convection. We find the influence of the Prandtl number to be significant; low Prandtl number fluids have a propensity for large-scale coherent vortex formation and slowly varying dynamics. Conversely, the high Prandtl case is dominated by significantly smaller length scales and more rapidly varying dynamics. However, both cases have zonal flows with similar strength, demonstrating that Reynolds stresses in high Prandtl number convection can be large when the buoyancy forcing is strong. By using a simple kinematic magnetic induction model we show that the structure of the magnetic field is not a direct indication of the underlying convective morphology when the magnetic diffusivity is large, as in Earth's core. Thus, our simulation results imply that the convective turbulence differs between thermally and chemically dominated convection, but that it may be difficult to determine the dominant forcing from geomagnetic field structure alone.

1. Introduction

The geomagnetic field is thought to be sustained by a combination of thermal and chemical convective turbulence within the Earth's liquid outer core (Buffett, 2000). As the inner core solidifies, chemical fractionation releases light elements at the inner core boundary (ICB) that results in chemical convection. Similarly, latent heating at the ICB and secular cooling of the Earth results in convection due to thermally buoyant core fluid. Thermal and chemical (or compositional) convection are distinct from one another due to their vastly different molecular diffusivities; the chemical diffusivity in the fluid outer core is thought to be approximately 10^3 times weaker than the thermal diffusivity (e.g. Braginsky and Roberts, 1995). Whereas studies have suggested that chemical convection is the dominant mechanism driving convection in the core (Lister and Buffett, 1995; Buffett et al., 1996), it is not yet clear as to how the structure and dynamics of thermal and chemical convection differ, and whether or not these differences have an observable signature in the geomagnetic field.

Molecular dynamic simulations find a kinematic viscosity and chemical diffusivity for Earth's liquid outer core to be $\nu \approx 10^{-6}$ m^2 s^{-1} and $\kappa_C \approx 5\times 10^{-9}$ m^2 s^{-1}, respectively (Alfé et al., 2000; Vočadlo et al., 2003). In contrast, estimates for the thermal diffusivity for the outer core give $\kappa_T \approx 6-7\times 10^{-6}$ m^2 s^{-1} (Stacey, 2007; Pozzo et al., 2012). These values can be recast in the form of a dimensionless ratio known as the Prandtl number, $Pr_{T,C}=\nu/\kappa_{T,C}$. Thus, the thermal Prandtl number is $Pr_T \sim \mathcal{O}(10^{-1})$, whereas the chemical Prandtl number (also known as the Schmidt number) is $Pr_C \sim \mathcal{O}(10^2)$. Neglecting differences in boundary conditions between thermal and chemical convection, the latter can be considered equivalently as high Prandtl number thermal convection and we take $Pr_{T,C}=Pr$.

The Prandtl number is known to control the *critical* wavenumber of fluid motion that is present near the onset of convection (Busse, 1970). The critical azimuthal wavenumber, m_{cr}, represents the scale at which fluid motion is forced when inertial effects are weak. The Reynolds number, $Re=UL/\nu$, where U and L are characteristic velocity and geometric length scales, respectively, is a measure of the relative effects of inertia and viscous forces in a given flow. For the Earth's core $U\sim 10^{-3}$ m s^{-1} and the outer core

* Corresponding author.
E-mail addresses: michael.calkins@colorado.edu (M.A. Calkins), jona@ess.ucla.edu (J.M. Aurnou), eldredge@seas.ucla.edu (J.D. Eldredge), keith.julien@colorado.edu (K. Julien).

0012-821X/$ - see front matter © 2012 Elsevier B.V. All rights reserved.
http://dx.doi.org/10.1016/j.epsl.2012.10.009

fluid layer depth is $L \approx 2300$ km, leading to $Re \sim 10^9$. As the forcing strength is increased, and the Reynolds number becomes large, fluid motion becomes characterized by a broad spectrum of wavenumbers (e.g. Tennekes and Lumley, 1972). Numerical simulations of convection in a spherical shell geometry suggest, however, that the most energetic motions remain in the vicinity of m_{cr} even as the Reynolds number becomes large (e.g. $Re \simeq 10^3$) (Gillet and Jones, 2006). This finding leads to the hypothesis that core turbulence is forced over two distinct wavenumber ranges corresponding to a thermally driven (i.e. low Prandtl number) component of core convection and a chemically driven (i.e. high Prandtl number) component of core convection.

Observations show that the geomagnetic field is dominantly dipolar, but it is also characterized by time-varying nonaxisymmetric coherent flux patches (e.g. Hulot et al., 2002; Finlay and Jackson, 2003; Jackson, 2003). Many three-dimensional dynamo studies have offered explanations for how such structures might be generated (Christensen et al., 1998; Aubert et al., 2008a,b). In general, they find that the viscous columnar structures that form near the onset of convection are able to generate dipolar magnetic fields that can be morphologically similar to the geomagnetic field (e.g. Christensen et al., 2010). However, computational constraints limit these simulations to parameter values that are extremely distant from those of the Earth's core. As a result, three-dimensional models are often dominated by viscous forces (e.g. Olson and Deguen, 2012) and are thus unlikely to correctly describe the dynamics of magnetic field generation under planetary core conditions. The large Reynolds number in the core suggests that turbulence plays an important role in determining geomagnetic field structure, whereas viscous forces are not likely to be relevant.

It is well known that the self-organization of turbulent fluid motions can result in the formation of coherent structures (e.g. Hussain, 1986). Coherent structures are characterized as fluid masses that possess like-signed vorticity (Hussain, 1986). Isolated vortices such as hurricanes in the Earth's atmosphere, and Jupiter's Great Red Spot (e.g. Marcus, 1993) are good examples of coherent structures. Recent simulations of rapidly rotating, plane-layer convective turbulence observe the formation of large-scale coherent vortices that are aligned with the rotation axis (Julien et al., 2012). It is thus possible that the coherent flux patches observed in the geomagnetic field are created by a similar mechanism.

The current work seeks to understand how the fluid properties, as represented by the Prandtl number, influence the convective dynamics and the potential for convective turbulence to form coherent vortices in a spherical shell, and whether these effects can be observed in the geomagnetic field. We use the quasi-geostrophic convection model (QGCM) to compare turbulent flows for two different Prandtl numbers, $Pr = 0.1$ and 10. The QGCM is a quasi-two-dimensional numerical model that allows for the investigation of more extreme parameter values than is possible in three-dimensional calculations; it is an extension of the asymptotic model originally developed by Busse (1970). Because the onset of convection is Prandtl number dependent we compare the two cases at a comparable Reynolds number. We then employ a simple kinematic model for the induction of the vertical component of a magnetic field to test whether thermal and chemical convection will generate distinct observable signatures in the geomagnetic field.

2. The quasi-geostrophic convection model

The QGCM employed in the current study is explained in detail in Calkins et al. (2012). Here we point out the general features and primary assumptions of the model. The equations of motion are solved in a cylindrical coordinate system (s,ϕ,z) in the equatorial plane of a spherical shell of inner radius r_i and outer radius r_o, rotating at a rate of Ω. Gravity is taken to vary linearly with cylindrical radius, $\mathbf{g} = -g\mathbf{s}$. The radius ratio used throughout this study is given by $\eta = r_i/r_o = 0.30$. No-slip, constant temperature boundary conditions are employed at the inner and outer boundaries, where T_i and T_o denote the temperatures at the respective boundaries. The equations are made dimensionless by employing $d = r_o - r_i$ as the length scale, d^2/κ as the time scale, and $\Delta T = T_i - T_o$ as the temperature scale. The dimensionless inner and outer radii are then given by $r_i = \eta/(1-\eta)$ and $r_o = 1/(1-\eta)$, respectively. The Proudman–Taylor theorem states that when the influence of rotation is strong enough, the radial and azimuthal velocities, u and v, respectively, remain invariant in the direction of the rotation axis (Greenspan, 1968). By continuity this implies that the vertical velocity, w, varies linearly in z, a central assumption made in the QGCM. It should be noted, though, that Gillet and Jones (2006) have shown that this linear dependence is only approximately observed in the limit of $E \to 0$ for the three-dimensional problem.

The nondimensional QGCM equations are then

$$\frac{1}{Pr}\left(\frac{\partial \zeta}{\partial t} + u\frac{\partial \zeta}{\partial s} + \frac{v}{s}\frac{\partial \zeta}{\partial \phi}\right) = \frac{2}{E}\frac{\partial w}{\partial z} - Ra\,\frac{\partial \theta}{\partial \phi} + \nabla^2 \zeta, \tag{1}$$

$$\nabla^2 \psi = -\zeta, \tag{2}$$

$$\frac{1}{Pr}\left(\frac{\partial \langle v \rangle}{\partial t} + \frac{1}{s^2}\frac{\partial}{\partial s}(s^2 \langle uv \rangle)\right) = -\frac{E^{-1/2} r_o^{1/2}}{h^{3/2}}\langle v \rangle + \nabla^2 \langle v \rangle - \frac{1}{s^2}\langle v \rangle, \tag{3}$$

$$\frac{\partial \theta}{\partial t} + u\frac{\partial \theta}{\partial s} + \frac{v}{s}\frac{\partial \theta}{\partial \phi} = -u\frac{dT_c}{ds} + \nabla^2 \theta, \tag{4}$$

where ζ is the axial vorticity, $\langle v \rangle$ is the ϕ-averaged azimuthal velocity, θ is the temperature perturbation, the half-height of the flow domain is $h(s) = \sqrt{r_o^2 - s^2}$ with slope $\partial_s h(s) = -s/\sqrt{r_o^2 - s^2}$, and the conductive temperature profile is given by $T_c(s) = \ln(s/r_o)/\ln(r_i/r_o)$. The streamfunction, ψ, is defined by the relations

$$u = \frac{1}{s}\frac{\partial \psi}{\partial \phi}, \tag{5}$$

$$v = -\frac{\partial \psi}{\partial s}. \tag{6}$$

The Ekman number and the Rayleigh number are denoted by $E = \nu/\Omega d^2$ and $Ra = \alpha \Delta T g d^3/\kappa \nu$, where α is the thermal expansivity. The Ekman number is the ratio of viscous forces to the Coriolis force, whereas the Rayleigh number is the strength of convective forcing. The first term on the right-hand side of Eq. (1) represents the effects of vortex stretching and is given by Schaeffer and Cardin (2005)

$$\frac{\partial w}{\partial z} = -\frac{2s}{h^2}u - \left(\frac{r_o E}{h^3}\right)^{1/2}\left(\zeta + \frac{s}{2h^2}v - \frac{s}{h^2}\frac{\partial u}{\partial \phi} + \frac{5 r_o s}{2h^3}u\right). \tag{7}$$

Eqs. (1)–(4) are time-stepped using a second-order Adams–Bashforth backward differentiation scheme, and discretized in space with second-order finite differences in radius and Fourier series in azimuth.

The zonal and nonzonal (i.e. convective) kinetic energies are defined, respectively, as $KE_z = 0.5[\langle v \rangle^2]_A$ and $KE_c = 0.5[\tilde{u}^2 + \tilde{v}^2]_A$, where $[\cdot]_A$ represents an average over the area of the flow domain, and $\tilde{u}$ and $\tilde{v} = v - \langle v \rangle$ are the nonzonal velocity components. Using these relations we define the zonal and convective Reynolds numbers as $Re_z = \sqrt{2\overline{KE}_z}/Pr$ and $Re_c = \sqrt{2\overline{KE}_c}/Pr$, where the overline, $\overline{(\cdot)}$, denotes a time-averaged quantity. For completeness, we

also include the time-averaged Nusselt number for each case, defined as

$$Nu = 1 + r_i \log\left(\frac{r_i}{r_o}\right)\frac{\partial\theta}{\partial s}\Big|_{r_i}.$$

3. Results

The linear equations were solved to determine the critical Rayleigh number, Ra_{cr}, and critical azimuthal wavenumber, m_{cr}, for the two Prandtl numbers used in the current study. The Ekman number is fixed at $E = 10^{-6}$. For $Pr = 0.1$ we found $Ra_{cr} = 1.7 \times 10^7$ and $m_{cr} = 18$ and for $Pr = 10$ we found $Ra_{cr} = 2.2 \times 10^8$ and $m_{cr} = 31$. Because Ra_{cr} depends on Pr, we choose to compare the two different Prandtl number cases at a comparable convective Reynolds number. In the results presented below, the convective Reynolds number is $Re_c \approx 3600$, whereas the zonal Reynolds numbers are $Re_z = 4874$ and $Re_z = 3451$ for $Pr = 0.1$ and $Pr = 10$, respectively. These values correspond to approximate supercriticalities (i.e. Ra/Ra_{cr}) of 18 for $Pr = 0.1$ and 455 for $Pr = 10$. Denoting N as the number of radial grid points and M as the number of Fourier modes, we used $N = 769$ and $M = 1856$ for $Pr = 0.1$, and $N = 1921$ and $M = 4992$ for $Pr = 10$. Note that even for comparable Reynolds numbers the $Pr = 10$ case required over six times the spatial resolution (i.e. $N \times M$) as the $Pr = 0.1$ case. The input and output parameters for both cases are given in Table 1.

Figs. 1a and 2a present snapshots of the vorticity for the $Pr = 0.1$ and $Pr = 10$ cases, respectively. Both cases show a significantly radial-dependent flow field, with narrow thermal plumes originating from the inner boundary and prograde-traveling thermal Rossby waves near the outer boundary, where the slope $\partial_s h(s) \to \infty$ as $s \to r_o$ and strong convective motions are suppressed. Also shown by the solid black curves are the instantaneous zonal flow profiles. Both cases exhibit similar zonal flow structure with a predominantly retrograde motion, and a weaker prograde flow near the outer boundary. At the Rayleigh numbers employed here, the time-averaged zonal flow is approximately 40% stronger for the low Pr case. Stokes' theorem relates the azimuthally averaged vorticity to the zonal flow strength as

$$\langle v \rangle = \frac{1}{s}\int_{r_i}^{s} s\langle \zeta \rangle \, ds. \tag{8}$$

By this relation we can conclude that the retrograde zonal flow observed near the inner boundary for both cases requires $\langle \zeta \rangle < 0$ in this region (Aubert et al., 2002, 2003). This effect is seen for the $Pr = 0.1$ case in Fig. 1a where ≈ 7 anticyclonic vortices are present. The dominant wavenumber in the retrograde zonal flow region is $m = 8$ for the $Pr = 10$ case, though the anticyclonic vortices are much less coherent due to the presence of small length scales in the flow.

Figs. 1b and 2b show the instantaneous temperature perturbations, where the azimuthally averaged value has been removed to improve visualization. For the $Pr = 0.1$ case the thermal structure is larger scale than the corresponding vortical structure shown in Fig. 1a. The opposite is true for the $Pr = 10$ case where the weaker thermal diffusivity results in finer thermal scales in comparison to the vorticity of Fig. 2a.

Table 1
Input and output parameters for the current study. Pr is the Prandtl number, N is the number of radial grid points, M is the number of azimuthal Fourier modes, E is the Ekman number, m_{cr} is the critical wavenumber, Ra_{cr} is the critical Rayleigh number, Ra is the Rayleigh number, Re_c is the convective Reynolds number, Re_z is the zonal Reynolds number, and Nu is the Nusselt number. See text for definitions.

Pr	N	M	E	m_{cr}	Ra_{cr}	Ra	Re_c	Re_z	Nu
0.1	769	1856	10^{-6}	18	1.7×10^7	3×10^8	3672	4874	3.93
10	1921	4992	10^{-6}	31	2.2×10^8	1×10^{11}	3637	3451	102.47

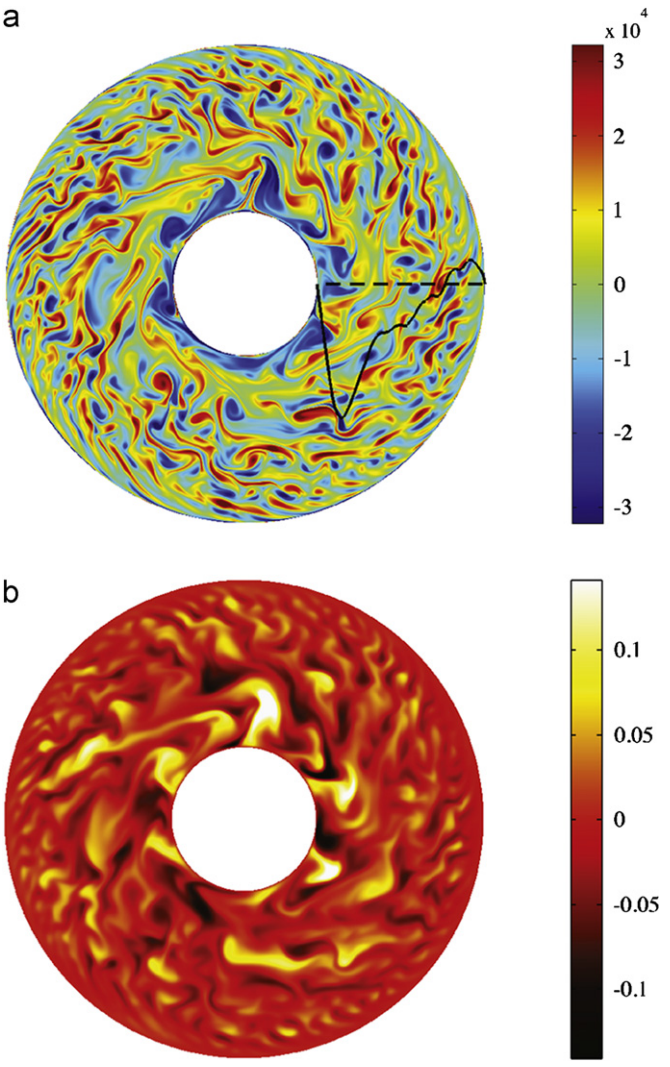

Fig. 1. Images of instantaneous: (a) vorticity and (b) modified temperature perturbation, $\theta - \langle\theta\rangle$, for $Pr = 0.1$. The instantaneous zonal flow profile is shown by the black solid curve in (a), where it has been normalized by the maximum absolute value ($|\langle v \rangle|_{max}/Pr = 11\,670$). The simulation parameters are given in Table 1.

To quantify the structural differences in the flow-field morphology for the two cases we compute the vorticity kurtosis, $Ku_\zeta = [\zeta - [\zeta]]_A^4 / [\zeta^2]_A^2$. The kurtosis is a measure of the occurrence of extreme values in a given quantity, and has thus been used traditionally in identifying the presence of coherent vortices in decaying (e.g. McWilliams, 1984) and forced (e.g. Maltrud and Vallis, 1991) two-dimensional turbulence. For reference, the kurtosis of the Gaussian distribution is 3 and the kurtosis of an exponential distribution is 6.

Fig. 3 shows the time evolution of the kurtosis for the two cases. The $Pr = 0.1$ case is characterized by a significantly higher time-averaged kurtosis of $\overline{Ku}_\zeta = 19.2$ in comparison to the $Pr = 10$ case with $\overline{Ku}_\zeta = 5.04$. These differences are consistent with the vorticity plots shown in Figs. 1a and 2a. For both cases, the flow structure is highly dependent upon radius; one-dimensional kurtosis calculations (i.e. integrating only in ϕ) showed that the vortical structures distributed azimuthally are of nearly identical size and shape. Note that because the kurtosis is a normalized quantity, the forcing scale (or critical wavenumber, m_{cr}) does not directly enter the calculation. Thus, differences in $\overline{Ku}_\zeta$ can be

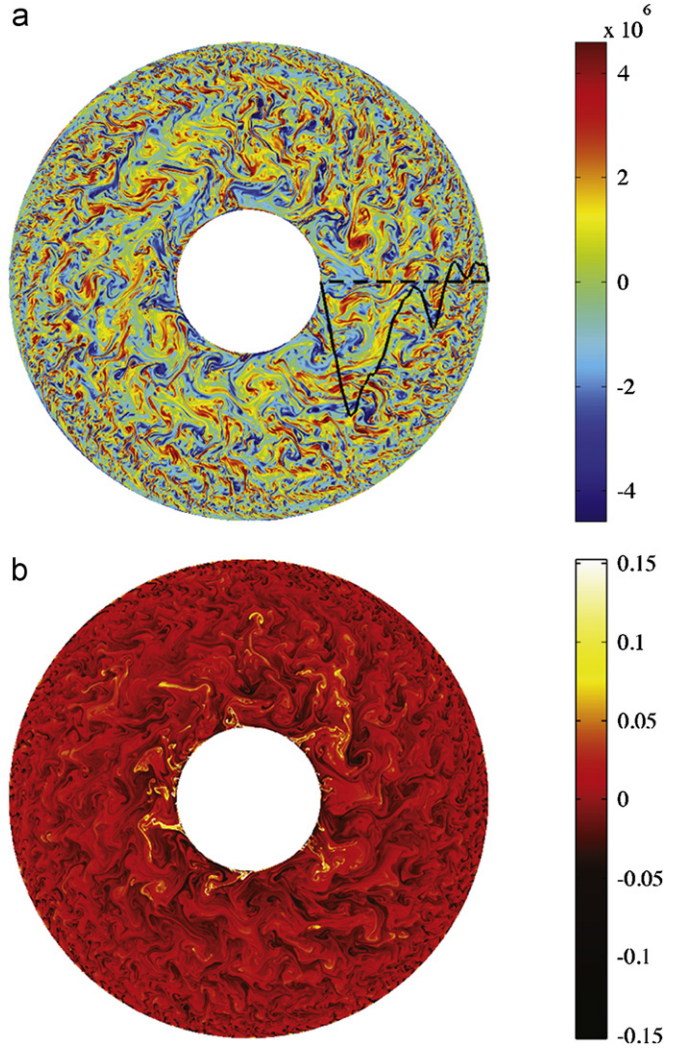

Fig. 2. Images of instantaneous: (a) vorticity and (b) modified temperature perturbation, $\theta - \langle\theta\rangle$, for $Pr = 10$. The instantaneous zonal flow profile is shown by the black solid curve in (a), where it has been normalized by the maximum absolute value ($|\langle v\rangle|_{max}/Pr = 9012$). The simulation parameters are given in Table 1.

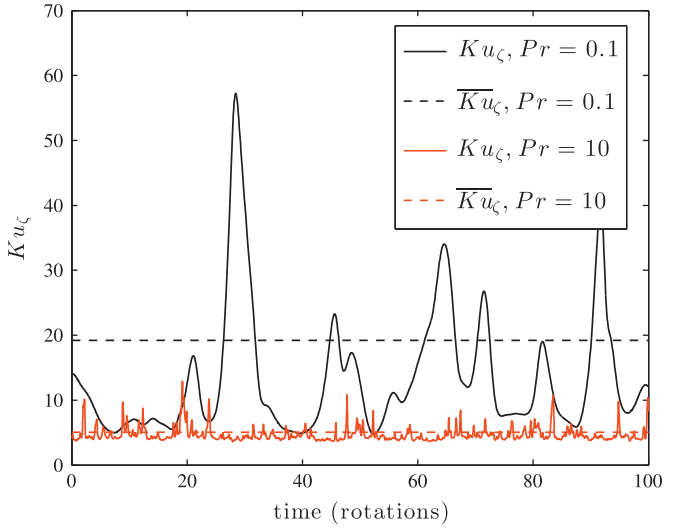

Fig. 3. Time variation of the vorticity kurtosis, Ku_ζ, for $Pr = 0.1$ (black line) and $Pr = 10$ (red line). The solid (dashed) lines show the instantaneous (time-averaged) vorticity kurtosis for each Prandtl number. (For interpretation of the references to color in this figure caption, the reader is referred to the web version of this article.)

attributed to dynamical differences, rather than simply differences in m_{cr}. It can be seen that the high Pr case exhibits rapid, low amplitude fluctuations in kurtosis due to the presence of small length scales in the flow field. The more slowly varying kurtosis observed in the $Pr = 0.1$ case is the result of the larger length scales present in the vorticity field, with anticyclonic vortex merging events generating the large, transient peaks in kurtosis.

3.1. Magnetic field structure

To determine how the convective flow structures in the core might influence the structure of the geomagnetic field we have performed simulations of a simple model that calculates the induced component of a vertical magnetic field (cf. Schaeffer and Cardin, 2006; Gillet et al., 2007a). This purely kinematic model assumes the flow is permeated by a uniform vertical magnetic field, B_0. The induced component b_z is then calculated according to the nondimensional equation

$$\frac{\partial b_z}{\partial t} + u\frac{\partial b_z}{\partial s} + \frac{v}{s}\frac{\partial b_z}{\partial \phi} = (1+b_z)\frac{\partial w}{\partial z} + \frac{Pr}{Pm}\nabla^2 b_z, \tag{9}$$

where we have used B_0 as the magnetic scale, and the magnetic Prandtl number is given by $Pm = v/\lambda$ with magnetic diffusivity λ. For the present study we employ $Pm = 0.03$ such that the magnetic Reynolds number $Rm = Re_c\, Pm \sim \mathcal{O}(100)$, similar to estimates for Earth's core. For the core, $Pm \sim \mathcal{O}(10^{-6})$, whereas three-dimensional numerical simulations typically employ $Pm \sim \mathcal{O}(1)$ due to computational constraints.

The magnetic induction is due entirely to the vortex stretching term, $\partial w/\partial z$, on the right-hand side of (9); as for the vorticity equation, this stretching term is calculated via (7). For simplicity we employ homogeneous Dirichlet boundary conditions on the induced magnetic field such that $b_z(r_i,\phi) = b_z(r_o,\phi) = 0$. The numerical methods used to solve Eq. (9) are identical to those used for the solution of Eqs. (1)–(4).

Fig. 4 presents the instantaneous views of the induced magnetic field at the same instant as the vorticity plots given in Figs. 1a and 2a. We see that whereas the morphological differences in the vorticity fields are clear, these differences become less pronounced in the structure of the induced magnetic field. This disparity in vortical and magnetic length scales is due to the relatively low magnetic Prandtl number employed here (cf. Soderlund et al., 2012, Fig. 2); the magnetic field is able to diffuse over the small scales present in the flow field. The kurtosis of the induced field, Ku_{b_z}, is shown in Fig. 5. The time-averaged magnetic field kurtosis for the $Pr = 0.1$ and $Pr = 10$ cases is $\overline{Ku}_{b_z} = 2.42$ and $\overline{Ku}_{b_z} = 2.01$, respectively. These similar kurtosis values demonstrate an important geophysical point: structural differences in the convective flow fields need not translate to similar structural differences in induced magnetic fields.

4. Discussion

We have presented a pair of simulations that demonstrate the importance of the fluid properties in controlling the morphology and dynamics of turbulent convection in a rotating spherical shell. The low Prandtl number case that we have investigated is representative of thermal convection in a liquid metal, whereas the high Prandtl case is representative of chemical convection. To allow for useful comparison between the thermal and chemical convection cases, the forcing strength (Ra) has been adjusted such that the typical convective velocities (Re_c) are approximately equal for the two cases. Both the high ($Pr = 10$; chemical) and low ($Pr = 0.1$; thermal) Prandtl cases exhibit zonal flows with comparable strength and similar

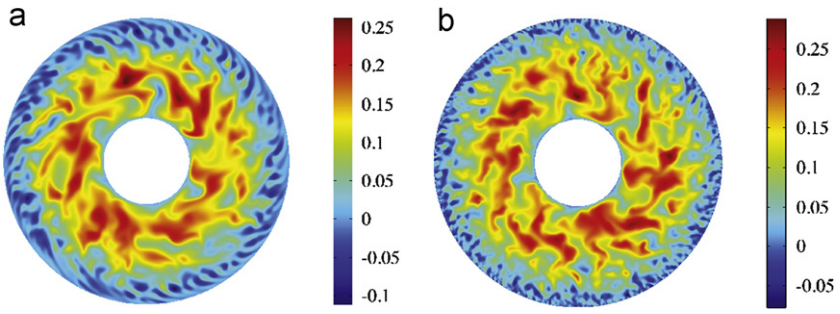

Fig. 4. Images of the instantaneous induced magnetic field for: (a) $Pr=0.1$ and (b) $Pr=10$. In both cases, $Pm=0.03$ such that $Rm=Re_cPm\approx 100$. The color scales have been shifted slightly for enhanced visualization.

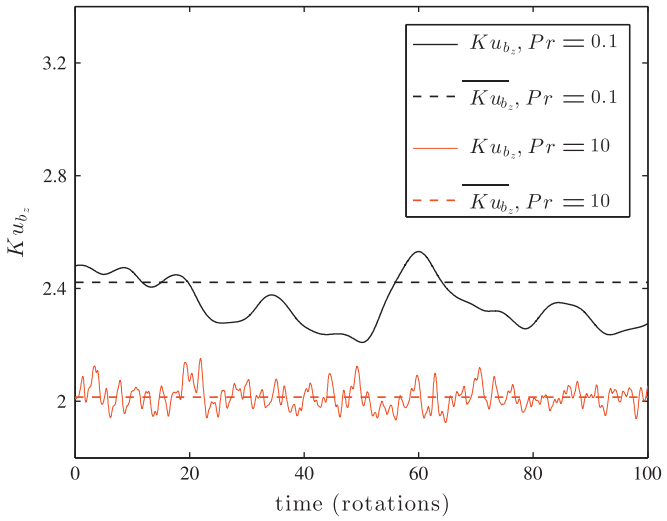

Fig. 5. Time variation of the induced magnetic field kurtosis, Ku_{b_z}, for $Pr=0.1$ (black line) and $Pr=10$ (red line). The solid (dashed) lines show the instantaneous (time-averaged) magnetic field kurtosis for each Prandtl number. (For interpretation of the references to color in this figure caption, the reader is referred to the web version of this article.)

structure. This observation demonstrates that Reynolds stresses can be large in high *Pr* fluids when the Rayleigh number is highly supercritical (as is thought to be the case in Earth's core). Morphologically, the high *Pr* case is characterized by the presence of significantly smaller length scales in comparison to the low *Pr* case. The vorticity kurtosis calculations show that the low *Pr* case possesses a greater propensity for coherent vortex formation with a mean value that is approximately four times that for the high *Pr* fluid. This tendency for higher vorticity kurtosis in the lower Prandtl number case may be due to the larger forcing scales (i.e. lower wavenumbers) present in low Prandtl number convection.

Both cases also show substantially different time dependences, with the low *Pr* case characterized by more slowly varying dynamics than the high *Pr* case. The observable temporal variations in the geomagnetic field are limited to annual timescales and longer (e.g. Finlay et al., 2010). In contrast, we were able to simulate less than 200 rotations after our runs equilibrated. These simulated time-series are not long enough to meaningfully compare against longer period geomagnetic secular variation signatures. Nevertheless, temporal statistics of geomagnetic secular variation may be useful in determining the dominant forcing mechanism in the core (e.g. Christensen et al., 2012).

From our convection simulation results alone, it is natural to conjecture that large-scale coherent flux patches in the geomagnetic field are generated from low Prandtl number convection. However, when viewed only through magnetic field measurements, our kinematic induction model shows that the effects of strong magnetic diffusion tend to remove the morphological differences between high and low *Pr* convection. Thus, when magnetic diffusion is strong (i.e. low *Pm*), as in planetary cores, our results indicate it will be difficult to discern between structural differences in the planetary magnetic field that are of thermal and/or chemical convective origin. The closeness of the magnetic field kurtosis for the two cases quantifies this behavior. Moreover, crustal filtering of the geomagnetic field only allows for the large-scale structure of the field to be observed, further hindering our ability to relate magnetic field structure to the underlying convective flow field.

Our results show that the value of the thermal (and chemical) diffusivity has a fundamental influence on the structure and dynamics of convective turbulence. Three-dimensional dynamo simulations have previously shown that the magnetic field structure is dependent upon the Prandtl number (e.g. Simitev and Busse, 2005), but, so far, have not made comparisons between cases with different Prandtl numbers at a comparable Reynolds number. Because the value of the thermal diffusivity selects the scales at which the fluid is forced, we conjecture that the structure and dynamics of convective turbulence will remain dependent on this value even for very high (i.e. planetary core-like) Reynolds numbers. A good example of this dependence is double-diffusive convection in the oceanic and astrophysical contexts where the diffusivities of both heat and solute play an important role in determining both the scales of fluid motion and the resulting dynamics (Traxler et al., 2011).

Furthermore, our finding that structurally and dynamically distinct flows arise due to differences in thermal diffusivity values suggests that the use of *turbulent* diffusivities in spherical shell convection is physically unrealistic. A reason that is cited commonly for employing $Pr=1$ in numerical simulations is that this value represents an effective turbulent Prandtl number whereby heat and momentum are transported equally throughout the fluid volume (e.g. Roberts and Aurnou, 2012). This equivalence in the transport of heat and momentum is known as the Reynolds analogy and has been shown to hold only in mechanically forced convection where buoyancy forces are negligible, and only for those cases for which *Pr* is already $\mathcal{O}(1)$ (Bejan, 1993).

The results presented here help to bridge the gap between three-dimensional models in which viscous forces are important (e.g. Soderlund et al., 2012), and the turbulent, rotationally constrained motions that characterize the Earth's core. Following recent three-dimensional models (Manglik et al., 2010; Breuer et al., 2010; Trümper et al., 2012), future work is required to examine the case in which both thermal and chemical buoyancy sources drive fully turbulent flows, and to determine how the convection dynamics and induced fields depend on the strength of each buoyancy force. Although the QGCM has been used to model kinematic three-dimensional magnetic fields (e.g. Schaeffer and Cardin, 2006; Gillet et al., 2007b), to date it has not been used

successfully for studying dynamos (e.g. Busse, 1975). Nevertheless, it has proven to be a valuable tool for advancing our understanding of planetary core physics by reaching parameter values that are not accessible to current three-dimensional models.

Acknowledgments

Michael A. Calkins gratefully acknowledges the financial support of a NSF EAR Postdoctoral Fellowship. Jonathan M. Aurnou and Keith Julien thank the NSF EAR CSEDI Program for support. All computations were carried out on NASA HEC's Pleiades supercomputer under award number SMD-09-1274. The authors would like to thank an anonymous referee for comments that greatly improved the manuscript.

References

Alfé, D., Kresse, G., Gillan, M.J., 2000. Structure and dynamics of liquid iron under Earth's core conditions. Phys. Rev. B 61 (1), 132–142.
Aubert, J., Jung, S., Swinney, H.L., 2002. Observations of zonal flow created by potential vorticity mixing in a rotating fluid. Geophys. Res. Lett. 29 (18), 1–4.
Aubert, J., Gillet, N., Cardin, P., 2003. Quasigeostrophic models of convection in rotating spherical shells. Geochem. Geophys. Geosyst. 4 (7), http://dx.doi.org/10.1029/2002GC000456.
Aubert, J., Amit, H., Hulot, G., Olson, P., 2008a. Thermochemical flows couple the Earth's inner core growth to mantle heterogeneity. Nature 454, 758–762.
Aubert, J., Aurnou, J.M., Wicht, J., 2008b. The magnetic structure of convection-driven numerical dynamos. Geophys. J. Int. 172, 945–956.
Bejan, A., 1993. Convection Heat Transfer. John Wiley & Sons, Inc.
Braginsky, S., Roberts, P., 1995. Equations governing convection in earth's core and the geodynamo. Geophys. Astrophys. Fluid Dyn. 79, 1–97.
Breuer, M., Manglik, A., Wicht, J., Trümper, T., Harder, H., Hansen, U., 2010. Thermochemically driven convection in a rotating spherical shell. Geophys. J. Int. 183, 150–162.
Buffett, B.A., 2000. Earth's core and the geodynamo. Science 288 (5473), 2007–2012.
Buffett, B.A., Huppert, H.E., Lister, J.R., Woods, A.W., 1996. On the thermal evolution of the Earth's core. J. Geophys. Res. 101 (B4), 7989–8006.
Busse, F.H., 1970. Thermal instabilities in rapidly rotating systems. J. Fluid Mech. 44, 441–460.
Busse, F.H., 1975. A model of the Geodynamo. Geophys. J. R. Astr. Soc. 42, 437–459.
Calkins, M.A., Noir, J., Eldredge, J.D., Aurnou, J.M., 2012. The effects of boundary topography on convection in Earth's core. Geophys. J. Int. 189, 799–814.
Christensen, U.R., Olson, P., Glatzmaier, G.A., 1998. A dynamo model interpretation of geomagnetic field structures. Geophys. Res. Lett. 25 (10), 1565–1568.
Christensen, U.R., Aubert, J., Hulot, G., 2010. Conditions for Earth-like geodynamo models. Earth Planet. Sci. Lett. 296, 487–496.
Christensen, U.R., Wardinski, I., Lesur, V., 2012. Timescales of geomagnetic secular acceleration in satellite field models and geodynamo models. Geophys. J. Int. 190, 243–254.
Finlay, C.C., Jackson, A., 2003. Equatorially dominated magnetic field change at the surface of Earth's core. Science 300, 2084–2086.
Finlay, C.C., Dumberry, M., Chulliat, A., Pais, M.A., 2010. Short timescale core dynamics: theory and observations. Space Sci. Rev. 155, 177–218.
Gillet, N., Jones, C.A., 2006. The quasi-geostrophic model for rapidly rotating spherical convection outside the tangent cylinder. J. Fluid Mech. 554, 343–369.
Gillet, N., Brito, D., Jault, D., Nataf, H.-C., 2007a. Experimental and numerical studies of convection in a rapidly rotating spherical shell. J. Fluid Mech. 580, 83–121.
Gillet, N., Brito, D., Jault, D., Nataf, H.-C., 2007b. Experimental and numerical studies of magnetoconvection in a rapidly rotating spherical shell. J. Fluid Mech. 580, 123–143.
Greenspan, H.P., 1968. The Theory of Rotating Fluids. Cambridge University Press, London.
Hulot, G., Eymin, C., Langlais, B., Mandea, M., Olsen, N., 2002. Small-scale structure of the geodynamo inferred from Oersted and Magsat satellite data. Nature 416, 620–623.
Hussain, A.K.M.F., 1986. Coherent structures and turbulence. J. Fluid Mech. 173, 303–356.
Jackson, A., 2003. Intense equatorial flux spots on the surface of the earth's core. Nature 424 (760–763).
Julien, K., Rubio, A.M., Grooms, I., Knobloch, E., 2012. Statistical and physical balances in low Rossby number Rayleigh–Bénard convection. Geophys. Astrophys. Fluid Dyn. 106 (4–5), 392–428.
Lister, J.R., Buffett, B.A., 1995. The strength and efficiency of thermal and compositional convection in the geodynamo. Phys. Earth Planet. Int. 91, 17–30.
Maltrud, M.E., Vallis, G.K., 1991. Energy spectra and coherent structures in forced two-dimensional and beta-plane turbulence. J. Fluid Mech. 228, 321–342.
Manglik, A., Wicht, J., Christensen, U., 2010. A dynamo model with double diffusive convection for mercury's core. Earth Planet. Sci. Lett. 289, 619–628.
Marcus, P.S., 1993. Jupiter's great red spot and other vortices. Ann. Rev. Astron. Astrophys. 31, 523–573.
McWilliams, J.C., 1984. The emergence of isolated coherent vortices in turbulent flow. J. Fluid Mech. 146, 21–43.
Olson, P., Deguen, R., 2012. Eccentricity of the geomagnetic dipole caused by lopsided inner core growth. Nat. Geosci. 5, 565–569.
Pozzo, M., Davies, C.J., Gubbins, D., Alfé, D., 2012. Thermal and electrical conductivity of iron at Earth's core conditions. Nature 485, 355–358.
Roberts, P.H., Aurnou, J.M., 2012. On the theory of core–mantle coupling. Geophys. Astrophys. Fluid Dyn. 106 (2), 157–230.
Schaeffer, N., Cardin, P., 2005. Quasigeostrophic model of the instabilities of the Stewartson layer in flat and depth-varying containers. Phys. Fluids 17 (104111).
Schaeffer, N., Cardin, P., 2006. Quasi-geostrophic kinematic dynamos at low magnetic Prandtl number. Earth Planet. Sci. Lett. 245, 595–604.
Simitev, R., Busse, F.H., 2005. Prandtl-number dependence of convection-driven dynamos in rotating spherical fluids shells. J. Fluid Mech. 532, 365–388.
Soderlund, K.M., King, E.M., Aurnou, J.M., 2012. The influence of magnetic fields in planetary dynamo models. Earth Planet. Sci. Lett. 333–334, 9–20.
Stacey, F.D., 2007. Core properties, physical. In: Gubbins, D., Herrero-Bervera, E. (Eds.), Encyclopedia of Geomagnetism and Paleomagnetism. Springer.
Tennekes, H., Lumley, J.L., 1972. A First Course in Turbulence. The MIT Press, Cambridge, MA.
Traxler, A., Garaud, P., Stellmach, S., 2011. Numerically determined transport laws for fingering (thermohaline) convection in astrophysics. Astrophys. J. Lett. 728 (L29).
Trümper, T., Breuer, M., Hansen, U., 2012. Numerical study of double-diffusive convection in the Earth's core. Phys. Earth Planet. Int. 194–195, 55–63.
Vočadlo, L., Alfé, D., Gillan, M.J., Price, G.D., 2003. The properties of iron under core conditions from first principles calculations. Phys. Earth Planet. Int. 140, 101–125.